

## **Regionalized tissue fluidization by an actomyosin cable is required for epithelial gap closure during insect gastrulation**

Jain A.<sup>1,2</sup>, Ulman V.<sup>1,3</sup>, Mukherjee A.<sup>4</sup>, Prakash M.<sup>1,5</sup>, Pimpale L.<sup>1,6</sup>, Muenster S.<sup>1,4,5,6</sup>, Panfilio K.A.<sup>7,8</sup>, Jug F.<sup>1,5</sup>, Grill S.W.<sup>1,5,6,9</sup>, Tomancak P.<sup>1,3</sup> and Pavlopoulos A.<sup>10</sup>

<sup>1</sup>Max-Planck-Institute of Molecular Cell Biology and Genetics, Dresden, Germany;

<sup>2</sup>Technische Universität Dresden, Dresden, Germany;

<sup>3</sup>IT4Innovations, Technical University of Ostrava, Czech Republic

<sup>4</sup>Max-Planck-Institute for the Physics of Complex Systems, Dresden, Germany;

<sup>5</sup>Center for Systems Biology, Dresden, Germany;

<sup>6</sup>Biotechnology Center, TU Dresden, Germany;

<sup>7</sup>Institute for Zoology: Developmental Biology, University of Cologne, Zùlpicher Str. 47b, 50674, Cologne, Germany

<sup>8</sup>School of Life Sciences, University of Warwick, Gibbet Hill Campus, Coventry, CV4 7AL, UK

<sup>9</sup>Cluster of Excellence Physics of Life, TU Dresden, Germany;

<sup>10</sup>Janelia Research Campus, Howard Hughes Medical Institute, Ashburn, United States

To whom correspondence shall be addressed: [tomancak@mpi-cbg.de](mailto:tomancak@mpi-cbg.de),  
[pavlopoulosa@janelia.hhmi.org](mailto:pavlopoulosa@janelia.hhmi.org)

## Abstract

Many animal embryos face early on in development the problem of having to pull and close an epithelial sheet around the spherical yolk-sac. During this gastrulation process, known as epiboly, the spherical geometry of the egg dictates that the epithelial sheet first expands and subsequently compacts to close around the sphere. While it is well recognized that contractile actomyosin cables can drive epiboly movements, it is unclear how pulling on the leading edge can lead to simultaneous tissue expansion and compaction. Moreover, the epithelial sheet spreading over the sphere is mechanically stressed and this stress needs to be dissipated for seamless closure. While oriented cell division is known to dissipate tissue stresses during epiboly in zebrafish, it is unclear how this is achieved in organisms that do not exhibit cell divisions during epiboly. Here we show that during extraembryonic tissue (serosa) epiboly in the red flour beetle *Tribolium castaneum*, the non-proliferative serosa becomes regionalized into two distinct territories: a dorsal region under higher tension away from the leading edge with larger, isodiametric and non-rearranging cells, and a more fluid ventral region under lower tension surrounding the leading edge with smaller, anisotropic cells undergoing cell intercalation. Our results suggest that fluidization of the leading edge is caused by a heterogeneous actomyosin cable that drives sequential eviction and intercalation of individual cells away from the serosa margin. Since this developmental solution utilized during epiboly resembles the mechanism of wound healing in other systems, we propose actomyosin cable-driven local tissue fluidization as a conserved morphogenetic module for closure of epithelial gaps.

# Main text

Epiboly is one of the evolutionarily conserved morphogenetic movements during animal gastrulation<sup>1</sup>. It involves spreading of an epithelial sheet over the spherical or ellipsoidal egg. The sheet eventually forms a continuous layer surrounding the embryo and the yolk sac entirely. During this morphogenetic event, fundamental geometrical and mechanical problems arise. First, in order to cover the entire egg, the epithelium has to expand in surface area. However, once the egg equator is reached, the expanding tissue must also undergo a regional compaction at its leading edge in order to seal seamlessly at the bottom of the sphere (**Fig 1A**). Second, spreading over a sphere induces mechanical stress in the tissue. Studies in fish showed that the tissue spreading is mediated by changes in cell area, cell number and cell arrangement coupled to constriction of an actomyosin ring in the yolk at the leading edge of the sheet<sup>2,3,4</sup>. However, it remains unclear how pulling forces at the leading edge can expand the cells in most of the tissue but not at the leading edge where cells must undergo a regional compaction. It has also been demonstrated for zebrafish that the tissue is under mechanical stress during epiboly and that the stress is released by oriented cell division<sup>4</sup>. In other epiboly systems however, cell division does not occur, and thus cannot alleviate built up stress.

For example, in many insect taxa, the developing embryo is completely surrounded by a protective epithelial cell layer of extraembryonic fate called serosa<sup>5,6</sup>. In the red flour beetle, *Tribolium castaneum*, extraembryonic serosa cells are initially specified as an anterior cap of the cellular blastoderm, which subsequently spreads over the gastrulating posterior embryonic part of the blastoderm<sup>7</sup>. This process resembles vertebrate epiboly but occurs in complete absence of serosa cell division (**Fig 1B**). The spreading serosa tissue expands around the equator at the posterior pole and eventually closes ventrally underneath the contracting embryo in a process known as serosa window closure<sup>8,9</sup>. It is not understood how the leading serosa cells surrounding the serosa window achieve compaction during window closure. It is also unknown if and how mechanical tension rises and dissipates in the serosa tissue during spreading.

To address these questions, we used the *Tribolium* serosa epiboly and closure as a model system to understand how the mechanical properties of cells and physical forces are regionalized to wrap a non-dividing epithelial sheet around an ellipsoidal egg. We imaged the progression of serosa spreading with multi-view light sheet microscopy in embryos expressing a nuclei-marking eGFP (**Fig 1C**, **Supplementary movie 1**). Taking advantage of the serosa topology as a superficial egg layer, we unwrapped the 3D data into 2D cartographic time-lapse projections and segmented the serosa part of the blastoderm tissue<sup>10</sup> (**Fig 1D**, **Supplementary Fig 1**, **Supplementary movie 2**). The serosa covered initially about 35% of the egg surface and spread to cover 100% of the surface (**Fig 1E**). In order to examine the expansion on the cellular level, we imaged embryos expressing LifeAct-eGFP and segmented all serosa cells at 5 reference stages during serosa expansion. We measured their surface area and plotted it onto the cartographic projection as a color map (**Fig 1G**). The results showed that the ~3-fold expansion in serosa surface was mirrored by an approximately 3-fold expansion of the apical area of serosa cells from stage 1 to stage 4 (**Fig 1F**). Strikingly, serosa cells did not expand uniformly; the apical area of ventral cells in the vicinity of the serosa window were on average

29% smaller compared to dorsal cells at stage 3 (**Fig 1F-G**). We conclude that serosa epiboly exhibits inhomogeneous apical cell area expansion in order to accommodate the ventral area compaction required by the elliptical geometry of the egg.

An alternative but not mutually exclusive mechanism to achieve ventral area compaction is by reducing the number of marginal cells (**Fig 2A**). It has been previously shown that the closure of epithelial holes in many instances of normal development and wound healing is accompanied by the exclusion of marginal cells from the leading edge<sup>2,3,11,12</sup>. While it is in principle possible that leading cells are not excluded and converge to a multicellular rosette, such a rosette has not been observed during *Tribolium* serosa window closure<sup>8,9,13</sup>. Our cell tracking experiments showed that the initial number of approximately 75 leading cells progressively decreased to only 5-6 cells during the final serosa closure (**Fig 2B,C**) and that these cells originated from all around the periphery of the window (**Fig 2D, Supplementary movie 3**). This observation suggested that cells must be leaving the edge of the serosa<sup>8</sup>. Indeed, careful examination of individual cells at the leading edge in time lapse recordings of embryos of a LifeAct-eGFP transgenic line revealed frequent rearrangement of cells through T1 transitions resulting in cells leaving the serosa edge (**Fig 2E,F, Supplementary movie 4**). The leaving cells shrunk their edge facing the serosa window and elongated radially in the direction approximately orthogonal to the window. Upon leaving the edge, the cells gradually relaxed to a hexagonal shape (**Supplementary Fig 2**). Mapping of those behaviours onto the time-lapse cartographic projections revealed that the serosa tissue was regionalized in two distinct territories. Dorsal cells several cell diameters away from the edge were regularly hexagonally packed and showed no neighbor exchanges. By contrast, ventral cells surrounding the serosa window deformed and frequently exchanged neighbors (**Fig 2H, Supplementary movie 5**). We quantified the propensity of the tissue to reconfigure through a shape index analysis<sup>14,15</sup>. The results showed that while dorsal cells had values around 3.8-3.9, which are indicative of a more solid tissue, ventral cells had significantly higher shape indices around 4.2 characteristic of more fluid tissues (**Fig 2G,H**). These results raised the hypothesis that during serosa epiboly the tissue in the vicinity of the window undergoes a solid-to-fluid structural transition (fluidization) that unjams the cell and enables seamless closure.

If the serosa tissue fluidizes along the dorsal ventral axis of the embryo during epiboly, we would expect spatiotemporal changes in tension of the serosa epithelium along this axis. To test this, we performed laser ablations inflicting large incisions across 3-4 cells at different reference stages and positions and compared the initial recoil velocities<sup>16,17</sup> (**Fig 3A,B**). The laser cutting experiments showed that the tension in the dorsal side increased progressively as the serosa expanded posteriorly and ventrally around the equator and plateaued after the serosa window formed (**Fig 3C**). Importantly, the tension in the ventral side closer to the window was lower compared to the dorsal side (**Fig 3D**). Thus, laser cutting experiments corroborate the regionalization of serosa into a more solid dorsal region that stays under high tension and a more fluid ventral region that has relaxed its tension.

Recent live imaging studies of *Tribolium* gastrulation suggested that an accumulation of actin, resembling a cable, emerges at the leading edge of the serosa<sup>9,18</sup>. To test whether this



accumulation indeed represents a contractile actomyosin cable, we injected mRNA encoding Tc.sqh-eGFP, which labels the *Tribolium* non-muscle myosin II (hereafter referred to as myosin), into *Tribolium* eggs before cellularization and imaged the embryos with multi-view light sheet microscopy. During epiboly, myosin accumulated at the boundary between the serosa and the embryonic primordium (that gives rise to the prospective embryo and another extraembryonic membrane, the amnion) (**Fig 4A, Supplementary movie 6**). Myosin enrichment at the serosa-embryonic boundary initiated shortly after epiboly started, and became more pronounced as the boundary stretched around the posterior pole. It peaked during serosa window closure and at this stage appeared as a contiguous supra-cellular cable (**Fig 4B**). The actomyosin cable lined the rim of the serosa window and underwent shape transformations from triangular to spherical shape during closure (**Fig 4A,B**). By segmenting and measuring the length and intensity of LifeAct accumulation, we found that the cable first increased its length until the leading serosa edge reached the apex at the posterior pole and then decreased in length to zero during window closure (**Fig 4C**). As the cable shrunk, the total myosin intensity normalized by cable length stayed the same or increased over time (**Fig 4D**). Laser cutting experiments of individual cell edges contributing to the serosa cable revealed that the actomyosin cable was under tension and that this tension increased over time (**Fig 4E,F,G, Supplementary movie 7**). Interestingly, individual cells of the cable appeared to contract their myosin loaded edges independently, as the recoil velocities of successive laser cuts of different edges in the same cable were comparable (**Fig 4H**). Moreover, the myosin distribution around the cable circumference showed strong heterogeneity, with some cells exhibiting higher and other cells exhibiting lower myosin accumulation. Cells with more myosin contracted their cable-forming edges and were evicted from the leading edge of the serosa earlier than cells with lower levels of myosin (**Fig 4I,J Supplementary movie 8**). Since the myosin intensity mirrors the cell leaving behavior, we conclude that differential line tension along the cable circumference drives the eviction of the cells from the cable and the resulting cell rearrangements lead to tissue fluidization and eventual closure of the epithelial gap (**Fig 4 K**).

Such a model predicts that in the absence of the actomyosin cable the serosa window will fail to close ventrally. Since the actomyosin cable forms at the extraembryonic/embryonic tissue boundary, we hypothesized that we could abolish its emergence by RNAi knockdown of the *Tribolium* transcription factor *zerknullt-1* gene (*Tc-zen1*) that prevents extraembryonic (serosal) cell fate specification<sup>7</sup>. Live imaging of *Tc-zen1* RNAi embryos injected with LifeAct-eGFP revealed indeed the absence of the actomyosin cable (**Fig 5A,B, Supplementary movie 9**). While such *Tc-zen1*<sup>RNAi</sup> embryos started the contraction and folding of the embryonic primordium as wild-type embryos, the epibolic movement halted and a ventral serosa window failed to form and close (**Fig 5A,B,E, Supplementary movie 9**). Compared to wild-type, the spreading cells in *Tc-zen1*<sup>RNAi</sup> embryos became larger, presumably due to their lower number (**Fig 5C**). The cells on the ventral leading edge, however, were much smaller (**Fig 5D**), did not elongate anisotropically (**Fig 5B**), did not exchange neighbors and were not evicted from the leading edge (**Fig 5E**). Finally, analysis of the shape index after *Tc-zen1* knock-down showed no differences between dorsal and ventral cells (**Fig 5H,I**). We conclude that in the absence of the actomyosin cable the marginal cells fail to become excluded from the leading edge, tissue

fluidization fails to occur and, consequently, the epithelial tissue fails to remodel and close its gap.

## Discussion

The epibolic expansion of *Tribolium* serosa to envelop the entire egg surface is a dynamic morphogenetic process constrained by the ellipsoidal geometry of the egg and the mechanical properties of the tissue. Our data suggest that the regionalized tissue fluidization at its leading edge, induced by an actomyosin cable, solves a number of problems associated with serosa epiboly. First, it addresses the geometric constraints necessitating both the expansion and regional compaction of the tissue to close the gap. Second, in the absence of patterned cell divisions, which have been implicated as a fluidization mechanism that promotes cell intercalation events<sup>19,20</sup>, local cell extrusion by actomyosin contractility is an alternative mechanism that powers cell intercalation and closure of this non-proliferative epithelium. Third, unjamming of the ventral cells releases mechanical stress in the serosa sheet, maintains epithelial integrity and promotes a seamless gap closure.

Previous studies have suggested that pulling forces exerted by the contractile cable reduce the circumference and eventually close the *Tribolium* serosa window with a purse string mechanism<sup>8,9</sup>. However, this model predicts increased tension in the tissue close to the cable<sup>4</sup> which contradicts our findings about the regionalization of the serosa. We measured smaller apical cell areas and a lower tension in the ventral serosa surrounding the cable as compared to the dorsal serosa further away from it. Imaging cable myosin dynamics with cellular resolution, together with the laser ablations, the *Tc-zen1* knock-down experiments and the shape index analyses, suggest that the contractile forces of the heterogeneous actomyosin network operate at the single-cell level to exclude marginal cells individually from the serosa window. The order in which cells are evicted is dictated by the local myosin accumulation at each cable-forming edge. It has been documented that myosin intensity correlates with contractility in wound healing cables<sup>21</sup> which is consistent with our finding that myosin intensity dictates cell eviction sequence. Furthermore, it has been suggested that a non-uniform stepwise contractility of individual edges is necessary for efficient epithelial closure during wound healing in *Drosophila* embryos and neural tube closure in chordates<sup>22</sup>. We propose that this kind of sequential contraction is also operating during window closure to dissipate serosa resistance built during each cycle of edge contraction.

Interestingly, there are more striking parallels between the closed actomyosin networks of the contracting *Tribolium* serosa window and the healing of *Drosophila* epithelial wounds. A recent study proposed that tissue fluidization is required for seamless wound healing in damaged *Drosophila* imaginal discs<sup>12</sup>. Similar to the actomyosin cable of the serosa window in *Tribolium*, the cable that assembles at the leading edge of the wound in *Drosophila* evicts cells from the wound periphery and promotes cell intercalation resulting in tissue fluidization and acceleration of epithelial gap closure. Taken together, these results point towards a conserved morphogenetic function of actomyosin cables in shaping and repairing epithelia by local tissue fluidization



## Acknowledgements:

We would like to thank Matthew A. Benton for kindly providing the pCS2+Lifeact-eGFP plasmid and sharing embryonic injection protocol and discussions, Sebastian Streichan for optimising ImSANE for *Tribolium* SPIM data and critical discussions, Alexander Dibrov for helping with tissue cartography cell segmentations, Christopher Schmied for optimising Snakemake SPIM data analysis pipeline for our datasets, Michaela Burkon for helping with *Tribolium* stock keeping and in doing parental RNAi experiments, Robert Haase and the MPI-CBG Image analysis facility for helping with image analysis, Mette Handberg-Thorsager and Yu-Wen Hsieh for sharing the pCS2+ Gap43-eYFP plasmid and helping with cloning, Ivana Viktorinova for schematic drawings, Anna Giles and Johannes Schinko (Averof lab), Peter Kitzmann (Bucher lab) and the van der Zee lab for sharing valuable transgenic lines, Siegfried Roth for critical discussions and Thorsten Horn for teaching various *Tribolium* techniques to A.J.

## Author Contributions

A.J. designed the research, performed experiments, analyzed the data, and wrote the manuscript. V.U produced image analysis software. A.M contributed to data analysis, M.P helped in segmenting data, L.P helped in laser ablation experiments, S.M contributed reagents and was involved in discussions, K.A.P. conducted RNAi parameter validation experiments and discussions, F.J. contributed to data segmentation, P.T. and A.P. conceived and oversaw the project, and wrote the manuscript.

## Methods

### *Tribolium* rearing and stocks

*Tribolium castaneum* stocks were kept at 32°C and 70% relative humidity on whole-grain or white flour supplemented with yeast powder according to standard procedures<sup>23</sup>. All mRNA injections were performed into embryos of the *vermilion*<sup>white</sup> strain. The following transgenic lines were used for live imaging: i) EFA-nGFP, ubiquitously expressing a nuclear-localized GFP reporter<sup>24</sup> (kindly provided by Michalis Averof's lab); ii)  $\alpha$ Tub-H2A-eGFP, ubiquitously expressing a nuclear eGFP reporter (kindly provided by Peter Kitzmann from Gregor Bucher's lab); EFA-Gap43-YFP,2A-Histone-RFP, ubiquitously expressing both a membrane YFP and a nuclear RFP reporter (kindly provided by Johannes Schinko and Anna Gilles from Michalis Averof's lab); iv)  $\alpha$ Tub-LifeAct-eGFP, ubiquitously labelling filamentous actin with eGFP<sup>25</sup> (kindly provided by the Van der Zee lab); v)  $\alpha$ Tub-Tc.sqh-eGFP, ubiquitously labelling the *Tribolium* non-muscle myosin II through its regulatory light chain (Tc-sqh). Details about the  $\alpha$ Tub-Tc.sqh-eGFP transgenesis construct are available upon request.

### RNA injections

Actin and myosin dynamics were also visualized in *vermilion*<sup>white</sup> embryos injected with in vitro transcribed capped mRNAs encoding LifeAct-eGFP or Tc-sqh-eGFP that were synthesized from linearized plasmid templates pT7-LifeAct-eGFP and pCS2+-Tc-sqh-eGFP, respectively<sup>9,18</sup>. For the RNAi knock-down experiments of *Tc-zen1*, the dsRNA against the *Tribolium zerknu*  $\square$  *lft-1* gene (TC000921) was obtained from the Eupheria Biotech company (iB\_03104) generating the dsRNAs for the iBeetle RNAi screen<sup>26</sup>. The mRNAs and the dsRNA were each injected at a final concentration of 1 mg/ml. Eggs from the *vermilion*<sup>white</sup> strain were collected for two hours at 30°C, aged for another hour at 30°C and dechorionated in 16% commercial bleach for 1 to 2 minutes. Dechorionated pre-blastoderm embryos were mounted on a 1% agar bed and were microinjected through their anterior pole under a brightfield upright microscope as previously described<sup>9,23</sup>. Injected eggs were incubated in humid chambers at 30°C for ~2 hours and the most homogeneously labeled and bright embryos were selected for imaging. For parental knock-down of *Tc-zen1* by RNAi, dsRNA was injected into the abdomen of female pupae collected from the  $\alpha$ Tub-LifeAct-eGFP transgenic line<sup>27</sup>. Injected adult females were crossed to males from the same line and their eggs were collected for imaging.

### Live imaging with confocal and light-sheet microscopy

Confocal live imaging was carried out at 25°C or 30°C on an inverted Zeiss LSM 780 system equipped with a temperature-controlled incubator. Embryos were mounted in 1% agarose in glass bottom petri dishes and covered in water. Embryos were scanned with a Zeiss 25x/0.8 NA Plan-Apochromat multi-immersion objective or a Zeiss 40x/1.2 NA C-Apochromat water-dipping objective with pixel sizes ranging between 0.2  $\mu$ m and 0.55  $\mu$ m, a z-step around 2  $\mu$ m and a temporal resolution of 5 minutes. Multi-view light-sheet imaging was carried out on a Zeiss Lightsheet Z.1 microscope equipped with a 20x/1.0 NA Plan Apochromat water-immersion detection objective and two 10x/0.2 NA dry illumination objectives. Embryos were embedded in glass capillaries in 1% low melting agarose dissolved in 1xPBS together with fluorescent beads as previously described<sup>28,29</sup>. For each embryo, z-stacks were acquired from 5 views every 72°

with voxel size 381  $\mu\text{m}$  x 381  $\mu\text{m}$  x 2  $\mu\text{m}$ . The starting point in the time-stamps used for all experiments was the last (12<sup>th</sup>) round of synchronous nuclear divisions which precedes the formation of the uniform blastoderm and all subsequent morphogenetic events<sup>9</sup>.

### **Laser ablations**

Laser ablations were performed either on an inverted Zeiss LSM 780 NLO with a 40x/1.2 NA water-dipping objective using an 800nm pulsed infrared laser or on a customized spinning disc confocal unit with a 63x water-dipping objective using an ultraviolet laser microdissection apparatus similar to the one described in <sup>30</sup> (custom setup Grill Lab). On the first system, three planes with 2 $\mu\text{m}$  z-spacing were imaged every 1.6 sec (Fig 3C, 4G), 0.5 Sec (Fig 3D), 2.5 sec (Fig 4H) and the cut was performed in the middle plane, while on the latter system a single plane was recorded every 0.5 second. Tissue cuts were about 12  $\mu\text{m}$  long spanning 3 to 4 cell diameters, while ablations of single edges were about 5  $\mu\text{m}$  long. The recoil velocity of ablated edges was measured between 6 post-cut time frames using the manual tracking plugin in Fiji and the initial recoil velocity was estimated using standard fitting procedures <sup>31</sup>.

### **Image processing**

The multi-view light-sheet datasets were registered and fused using Fiji plugins as previously described<sup>32-34</sup>. The 4D (3D+time) fused datasets were converted into 3D (2D+time) time-lapse maps by making cylindrical projections using the ImSANE software<sup>10</sup>. Distortions that are inherent to the mapping of curved surfaces onto a plane were corrected with custom Fiji plugins (available on the "Tomancak lab" Fiji update site) thereby allowing the measurement of quantities like size, shape, shape factor, density and velocity. Nuclei in the depth color-coded cartographic projections were tracked using MaMuT and Mastodon (Wolff eLife 2018; <http://sites.imagej.net/Mastodonpreview/>).

# References

1. Solnica-Krezel, L. Conserved patterns of cell movements during vertebrate gastrulation. *Curr. Biol.* **15**, R213–28 (2005).
2. Keller, R. E. & Trinkaus, J. P. Rearrangement of Enveloping Layer Cells Without Disruption of the Epithelial Permeability Barrier as a Factor in Fundulus Epiboly. *Developmental Biology* **120**, 12–24 (1987).
3. Koppen, M. Coordinated cell-shape changes control epithelial movement in zebrafish and *Drosophila*. *Development* **133**, 2671–2681 (2006).
4. Campinho, P. *et al.* Tension-oriented cell divisions limit anisotropic tissue tension in epithelial spreading during zebrafish epiboly. *Nat Cell Biol* **15**, 1405–1414 (2013).
5. Panfilio, K. A. Extraembryonic development in insects and the acrobatics of blastokinesis. *Developmental Biology* **313**, 471–491 (2008).
6. Schmidt-Ott, U. & Kwan, C. W. Morphogenetic functions of extraembryonic membranes in insects. *Curr Opin Insect Sci* **13**, 86–92 (2016).
7. van der Zee, M., Berns, N. & Roth, S. Distinct Functions of the *Tribolium* zerknullt Genes in Serosa Specification and Dorsal Closure. *Current Biology* **15**, 624–636 (2005).
8. Handel, K., Grünfelder, C. G., Roth, S. & Sander, K. *Tribolium* embryogenesis: a SEM study of cell shapes and movements from blastoderm to serosal closure. *Dev Genes Evol* **210**, 167–179 (2000).
9. Benton, M. A., Akam, M. & Pavlopoulos, A. Cell and tissue dynamics during *Tribolium* embryogenesis revealed by versatile fluorescence labeling approaches. *Development* **140**, 3210–3220 (2013).
10. Heemskerk, I. & Streichan, S. J. Tissue cartography: compressing bio-image data by dimensional reduction. *Nature Methods* 1–5 (2015).
11. Wood, W. *et al.* Wound healing recapitulates morphogenesis in *Drosophila* embryos. *Nat Cell Biol* **4**, 907–912 (2002).
12. Tetley, R. J. *et al.* Tissue fluidity promotes epithelial wound healing. *Nat Phys* (2019).
13. Benton, M. A. *Analysis of embryonic development in Tribolium castaneum using a versatile live fluorescent labelling technique.* (2013).
14. Bi, D., Yang, X., Marchetti, M. C. & Manning, M. L. Motility-Driven Glass and Jamming Transitions in Biological Tissues. *Phys. Rev. X* **6**, 021011–13 (2016).
15. Yang, X. *et al.* Correlating cell shape and cellular stress in motile confluent tissues. *Proc. Natl. Acad. Sci. U.S.A.* **114**, 12663–12668 (2017).
16. Smutny, M., Behrndt, M., Campinho, P., Ruprecht, V. & Heisenberg, C.-P. in *Quantitative Image Analysis of Cell Behavior and Molecular Dynamics During Tissue Morphogenesis* **1189**, 219–235 (Springer New York, 2014).
17. Rauzi, M. & Lenne, P.-F. *Cortical Forces in Cell Shape Changes and Tissue Morphogenesis. Cellular Adhesion in Development and Disease* **95**, 93–144 (Elsevier Inc., 2011).
18. Münster, S. *et al.* Attachment of the blastoderm to the vitelline envelope affects gastrulation of insects. *Nature* **568**, 395–399 (2019).
19. Firmino, J., Rocancourt, D., Saadaoui, M., Moreau, C. & Gros, J. Cell Division Drives Epithelial Cell Rearrangements during Gastrulation in Chick. *Developmental Cell* **36**, 249–261 (2016).
20. Petridou, N. I., Grigolon, S., Salbreux, G., Hannezo, E. & Heisenberg, C.-P. Fluidization-mediated tissue spreading by mitotic cell rounding and non-canonical Wnt signalling. *Nat Cell Biol* **21**, 169–178 (2019).



21. Fernandez-Gonzalez, R., de Matos Simoes, S., ROper, J.-C., Eaton, S. & Zallen, J. A. Myosin II Dynamics Are Regulated by Tension in Intercalating Cells. *DEVCEL* **17**, 736–743 (2009).
22. Zulueta-Coarasa, T. & Fernandez-Gonzalez, R. Dynamic force patterns promote collective cell movements during embryonic wound repair. *Nat Phys* 1–15 (2018).
23. Brown, S. J. *et al.* The Red Flour Beetle, *Tribolium castaneum* (Coleoptera): A Model for Studies of Development and Pest Biology. *Cold Spring Harbor Protocols* **2009**, pdb.emo126–pdb.emo126 (2009).
24. Sarrazin, A. F., Peel, A. D. & Averof, M. A Segmentation Clock with Two-Segment Periodicity in Insects. *Science* **336**, 338–341 (2012).
25. van Drongelen, R., Theoretical, T. V.-F. J. O.2018. Mechanics of epithelial tissue formation. *Elsevier* (2018)
26. Schmitt-Engel, C. *et al.* The iBeetle large-scale RNAi screen reveals gene functions for insect development and physiology. *Nature Communications* **6**, 1–10 (2015).
27. Bucher, G., Scholten, J., Biology, M. K. C.2002. Parental mai in *Tribolium* (coleoptera). *Cell* (2002).
28. Schmied, C. & Tomancak, P. Sample Preparation and Mounting of *Drosophila* Embryos for Multiview Light Sheet Microscopy. *Methods Mol. Biol.* **1478**, 189–202 (2016).
29. Wolff, C. *et al.* Multi-view light-sheet imaging and tracking with the MaMuT software reveals the cell lineage of a direct developing arthropod limb. *eLife* 34410.00, (2018)
30. Grill, S. W., Gönczy, P., Stelzer, E. H. K. & Hyman, A. A. Polarity controls forces governing asymmetric spindle positioning in the *Caenorhabditis elegans* embryo. *Nature* **409**, 630–633 (2001).
31. Mayer, M., Depken, M., Bois, J. S., Jülicher, F. & Grill, S. W. Anisotropies in cortical tension reveal the physical basis of polarizing cortical flows. *Nature* **467**, 617–621 (2010).
32. Preibisch, S., Saalfeld, S., Schindelin, J. & Tomancak, P. Software for bead-based registration of selective plane illumination microscopy data. *Nature Publishing Group* **7**, 418–419 (2010).
33. Schindelin, J. *et al.* Fiji: an open-source platform for biological-image analysis. *Nature Methods* **9**, 676–682 (2012).
34. Schmied, C., Steinbach, P., Pietzsch, T., Preibisch, S. & Tomancak, P. An automated workflow for parallel processing of large multiview SPIM recordings. *Bioinformatics* **32**, 1112–1114 (2016).

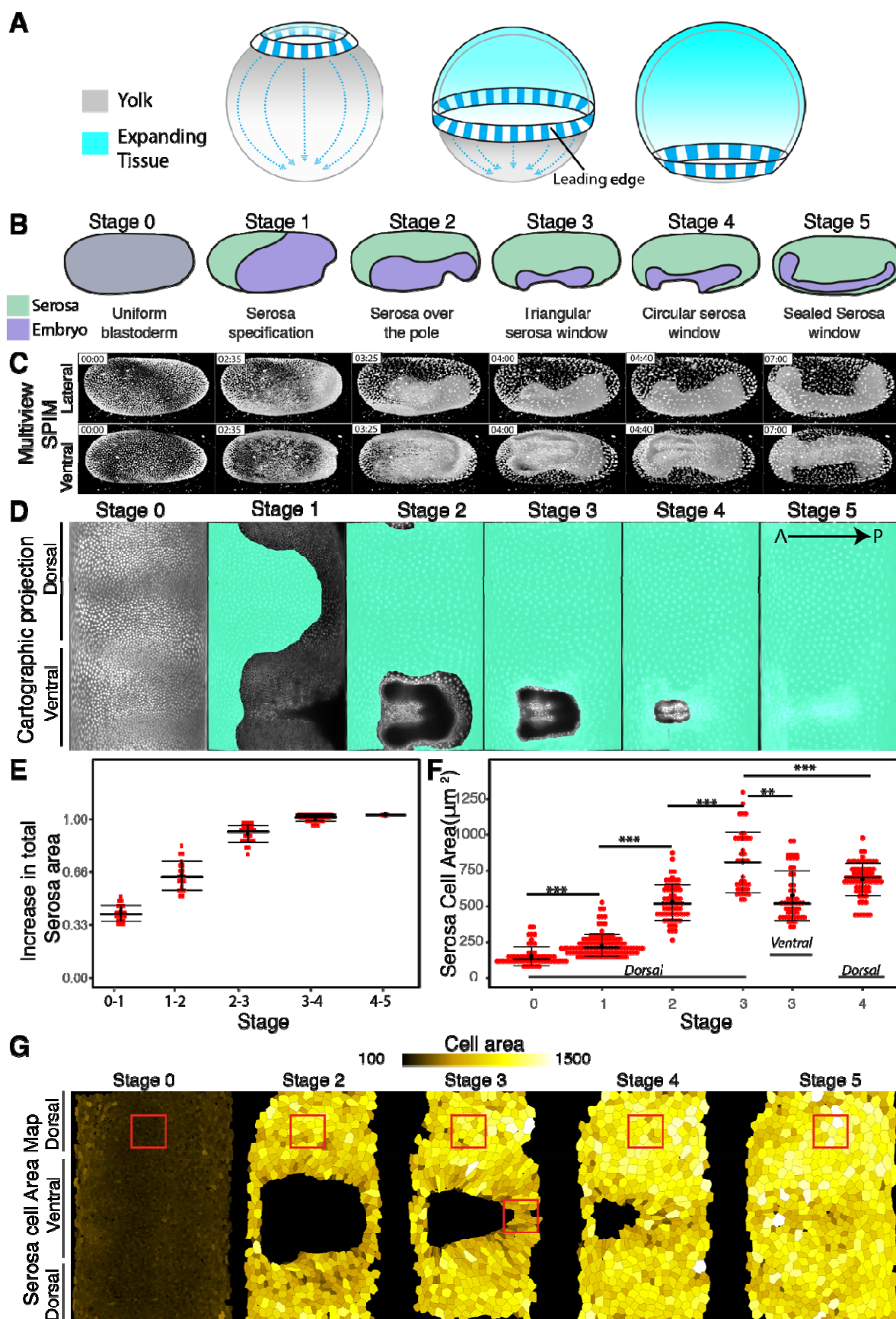


# Figure 1: Inhomogeneous tissue expansion during *Tribolium* serosa morphogenesis.

(A) Schematic depiction of the geometric constraints experienced by a tissue expanding over a spherical yolk cell. The leading edge undergoes an area increase followed by an area decrease after it crosses the equator.

(B) Illustrations of the stages of *Tribolium* embryogenesis from cellular blastoderm to serosa window closure. The domains of blastoderm adopting the extraembryonic (serosa) and embryonic fates are indicated by color.

(C) Maximum intensity projections of reconstructed multi-view time-lapse SPIM recording of a *Tribolium* embryo expressing fluorescent EFA:nGFP nuclear marker. The embryo is shown from the lateral and ventral view at the 6 reference stages corresponding to the schematics in (B).

(D) 2D cartographic projection of a 4D SPIM recording of *Tribolium* embryo expressing EFA:nGFP. The extent of the serosa tissue is highlighted in green.

(E) The area of the serosa tissue calculated from cartographic projections of 4D SPIM recordings. The data are normalized to the total serosa area at stage 5 in each case. For every stage the total serosa area is calculated for all timepoints between two consecutive stages in three different embryos and plotted as a distribution.

(F) Comparison of the distributions of apical areas of cells sampled from point scanning confocal recordings of *Tribolium* embryos expressing LifeAct-eGFP membrane marker at reference stages labeled according to (B). The difference between distributions was tested using parametric t-test. P-values between 0.009-0.001 are labeled with \*\* and <0.001 with \*\*\*. The number of cells (n) and the number of embryos (N) sampled at different stages were as follows: Stage 0 n=58, N=6, Stage 1 n=72, N=4, Stage2 n=65, N=6, Stage 3 n=79, N=4, Stage 4 n=77, N=8.

(G) Cartographic projections of reference stages of an embryo labelled with LifeAct-eGFP and imaged live with multi-view SPIM. The projections are overlaid with manually curated automated segmentation results visualizing apical areas of serosa cells through a color code. Red boxes indicate the approximate regions from which cells were sampled in confocal datasets quantified in (H).



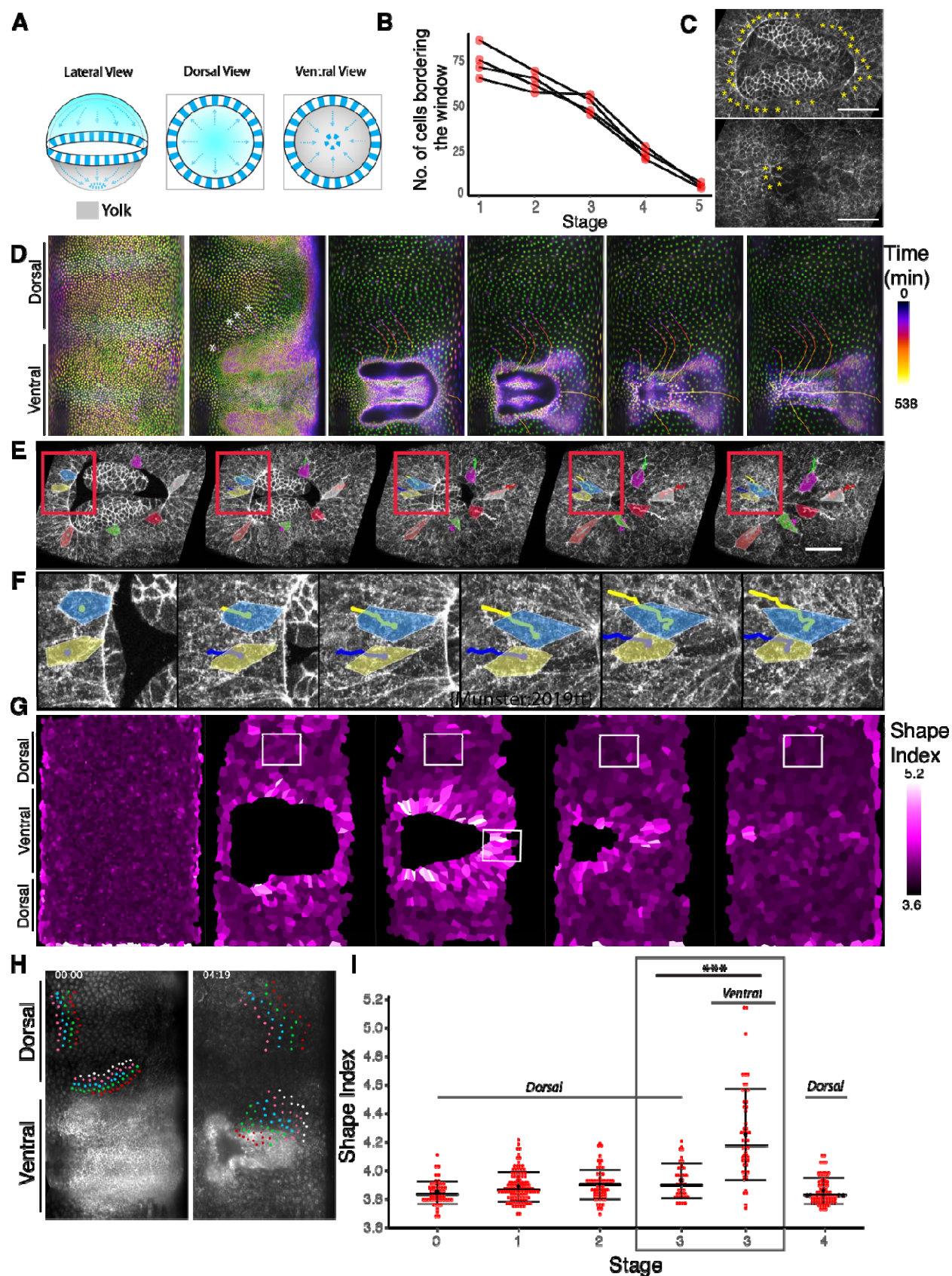


**Figure 2: Cell behaviors at the ventral leading edge of the serosa window are distinct from the dorsal serosa.**

- (A) Schematic illustration of the putative mechanism of closing serosa window by reducing the number of cells at the leading edge of the window over time.
- (B) Plot of the total number of cells at the embryo-serosa boundary during serosa window closure counted at the five reference stages. (n=4)
- (C) Confocal images highlighting the cells (stars) forming the leading edge of the serosa window at Stage 3 and Stage 5.
- (D) Cartographic projection of a Histone-eGFP labelled embryo imaged with multiview SPIM. The progressively deeper onion layers of the projection are color-coded to distinguish superficial and internal nuclei. The nuclei participating in closing of the serosa window were back-tracked to the uniform blastoderm stage to reveal their spatial origin.
- (E) Frames from a confocal recording of the serosa window closure in embryos expressing LifeAct-eGFP. Selected cells at the leading edge of the serosa window are outlined and colored to show that some cells shrink their serosa window facing membranes and planarly intercalate into the serosa epithelium. Red box marks the inset shown in (F).
- (G) Cartographic projections of an embryo labelled with LifeAct-eGFP, imaged in SPIM and semi-automatically segmented. The color code indicates the value of the shape Index for each segmented serosa cell.
- (H) Cartographic projections of an embryo labelled with LifeAct-eGFP at the beginning and towards the end of serosa window closure. Selected cells were tracked over time and color coded to visualize the difference in the extent of neighbor exchanges between the dorsal cells and ventral cells close to the leading edge of the serosa window.
- (I) Distributions of shape factors of cells segmented from Stage 0-4 LifeAct-eGFP embryos imaged by point scanning confocal. The measurements were done in regions corresponding to the white boxes in (G). The shape index distributions of stage 3 dorsal and ventral cells are significantly different (p-value <0.001 marked with \*\*\*). The other distributions are not significantly different. Numbers of cells and embryos are the same as 1F.

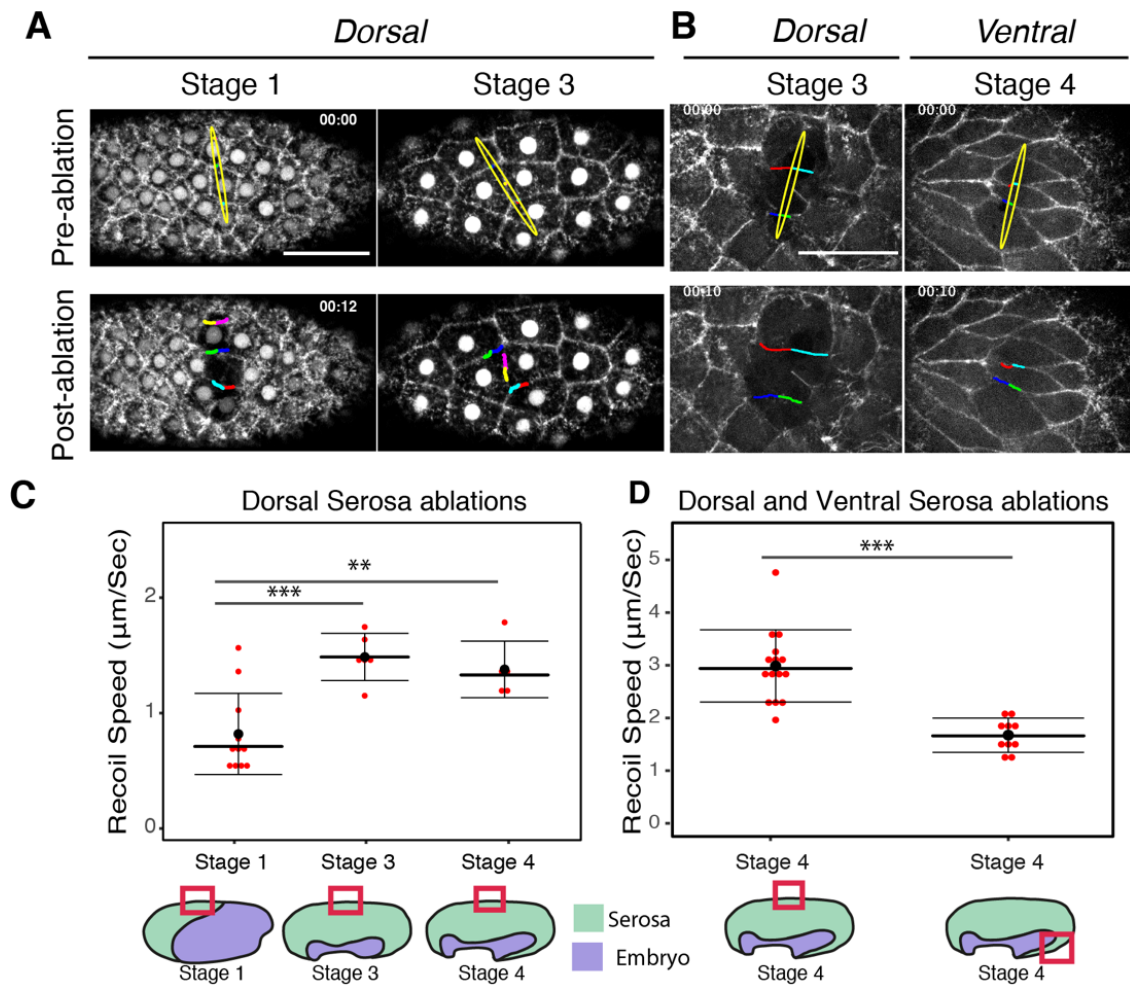


**Figure 3: Tension landscape in the expanding serosa**

(A) Images show the tissue before and after laser ablation of the serosa in the dorsal region of the embryo expressing LifeAct-eGFP and EFA:nGFP at Stage 1 and Stage 3. The yellow ellipse shows the extent of the cut. The colored lines highlight the displacement of the severed cell edges. Scale bar is 50 micrometers.

(B) Comparison of laser ablation in dorsal and ventral regions of the serosa (as depicted schematically below the graph in (D)) at stages 3 and 4 in distinct embryos expressing LifeAct-eGFP. The yellow ellipse shows the extent of the cut.

(C) Graph shows comparison of recoil velocities after laser ablation at Stages 1, 3 and 4. The ablations were performed at the same dorsal position of each embryo as indicated by the reference stage schematics below.

(D) Graph shows comparison of recoil velocities after laser ablation of serosa cells in the dorsal and the ventral regions of Stage 3 embryos.

(C,D) Error bars show standard deviations. The pairwise differences in distributions is tested using t-test and p-values between 0.009-0.001 are labeled with \*\* and <0.001 with \*\*\*.



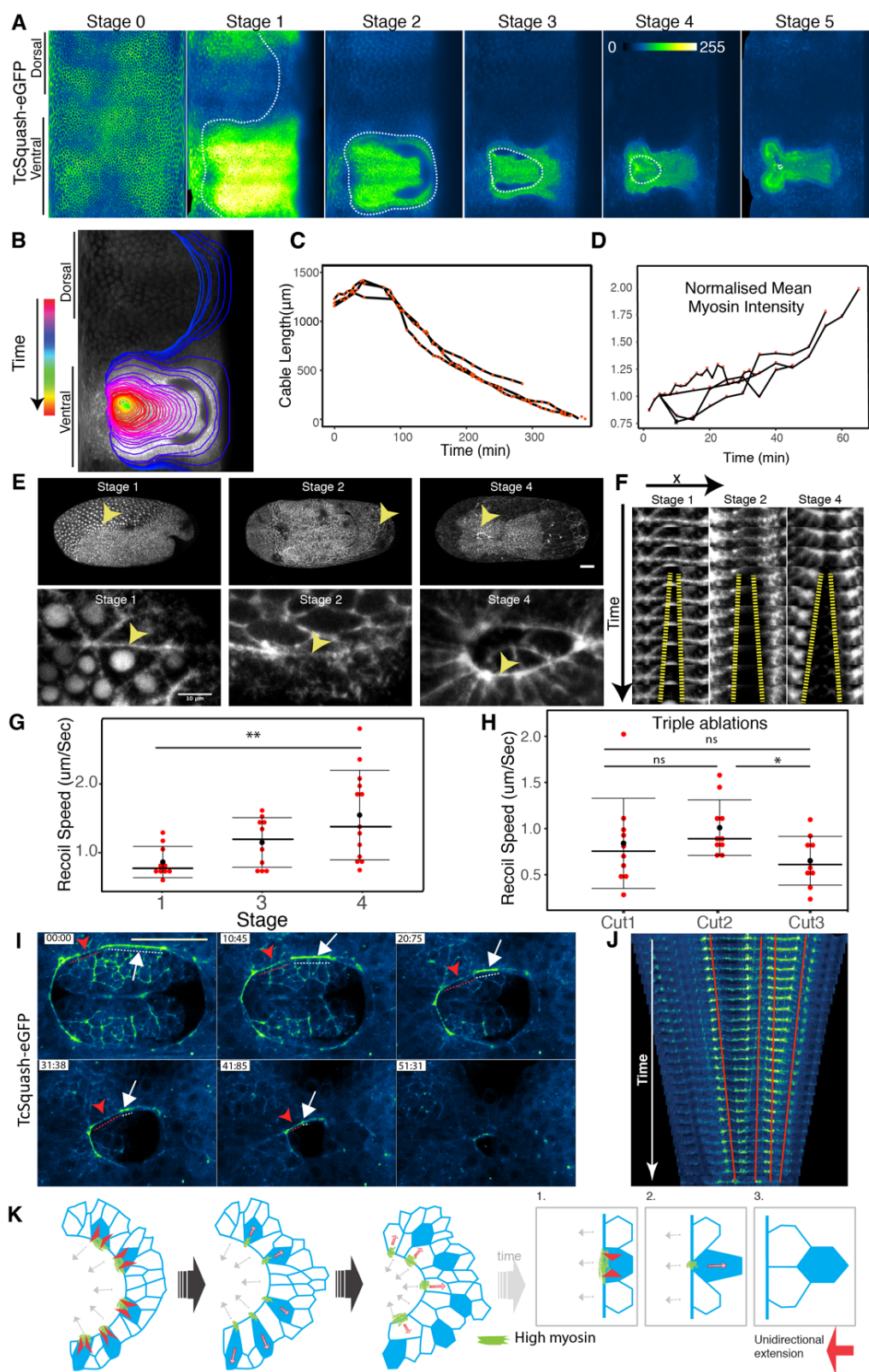




**Figure 4: Actomyosin forms a contractile supracellular cable at the embryo-serosa boundary that promotes tissue fluidization.**

(A) Cartographic projection of *Tribolium* embryos injected with Tc-sqh-eGFP and imaged with multiview SPIM. The accumulation of myosin at the border between serosa and embryos is highlighted by the dotted line.

(B) The shape of the supracellular actomyosin cable imaged as in (A) is outlined over time as it emerges dorsally and closes on the ventral side of the embryo. The color of the outline corresponds to the time stamp of the frame from which it was traced.

(C) The graph shows the length of manually segmented actomyosin cable as a function of time during serosa window closure. (n=3)

(D) The graph shows normalized mean myosin intensity at the manually segmented cable over time. (n=4)

(E) Maximum intensity projections of confocal stacks of Tc.sqh-eGFP injected embryos from 3 different developmental stages. Arrows points to the regions of the cable that was ablated. Bottom row shows close ups of areas marked by arrows in top row. Scale bar in top panel is 50 $\mu$ m.

(F) Kymograph of the recoiling membrane edges after laser ablation of the cells forming the actomyosin cable at the leading edge of the serosa window.

(G) The distributions of recoil velocities after ablation of the cable forming cells at different stages. Error bars indicate standard deviation. The pairwise differences in distributions is tested using t-test and significant p-value between 0.009-0.001 is labelled with \*\*. The number of cut embryos is >10 in each case.

(H) The distributions of recoil velocities after three successive laser ablations of three distinct cells in the same cable. Error bars indicate standard deviation. The pairwise differences in distributions is tested using t-test and significant p-value between 0.05-0.01 is labelled with \* and ns corresponds to not significant. The number of cut embryos is >10 in each case.

(I) Images from a timelapse point scanning confocal recording of an embryo expressing Tc.sqh-eGFP. Myosin localization at the cable is different between different cable forming cells. Cell with high myosin accumulation is labelled with white arrow and its extent is highlighted with white dotted line. Cell with low myosin is labelled similarly but in red.

(J) Kymograph of myosin cable shown in (I). The cable was segmented manually and straightened using Fiji plugins. Regions of the cable with high myosin are shrinking faster compared to regions with low myosin.

(K) Illustration shows the differential contraction of the serosa-window-facing cell edges depending on the amount of myosin. This leads to T1 transitions in the serosa (right). As a result, the leading edge of serosa extends unidirectionally and at the same time undergoes structural rearrangement. Green color depicts the myosin enriched in the contracting cells.

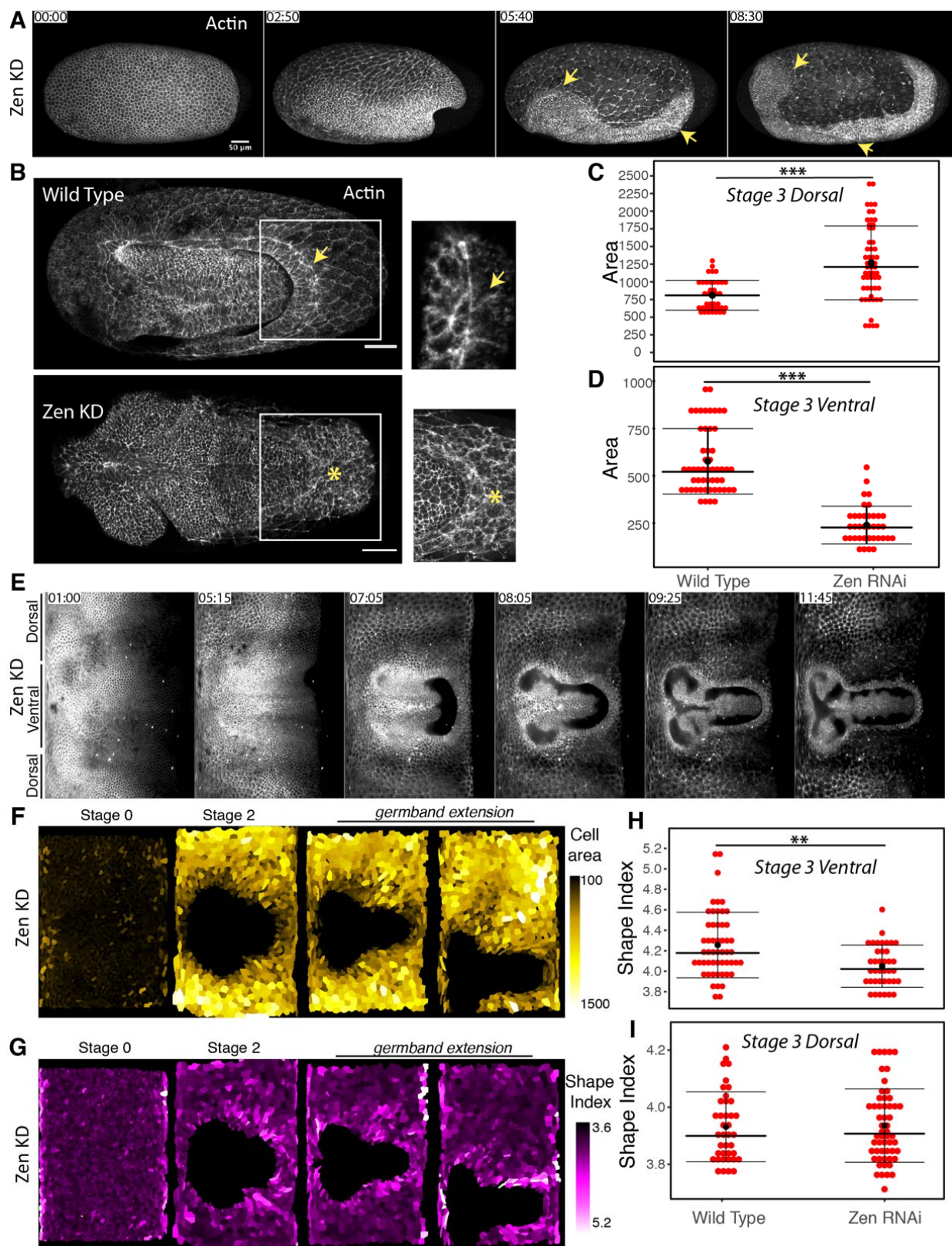


**Figure 5: Cell and tissue dynamics in *Tc-zen1* knockdown embryos**

(A) Maximum intensity projections of a developing embryo labelled with LifeAct-GFP, injected with dsRNA for *Tc-zen1* and imaged with point scanning confocal microscope. Arrows point to the open serosa window in the head and the posterior region.

(B) Selected maximum intensity projection images from wildtype and *Tc-zen1* RNAi embryos at stage 3. Inset shows the cable in wildtype embryos (arrow) and absence of the cable in the knockdown (\*). Scale bar is 50 micrometers.

(C) The distributions of cell areas in wildtype and *Tc-zen1* knockdown embryos sampled from confocal datasets in the ventral (C) and dorsal (D) serosa regions at Stage 3. The differences in distributions were tested using t-test and p-values <0.001 are labeled with \*\*\*.

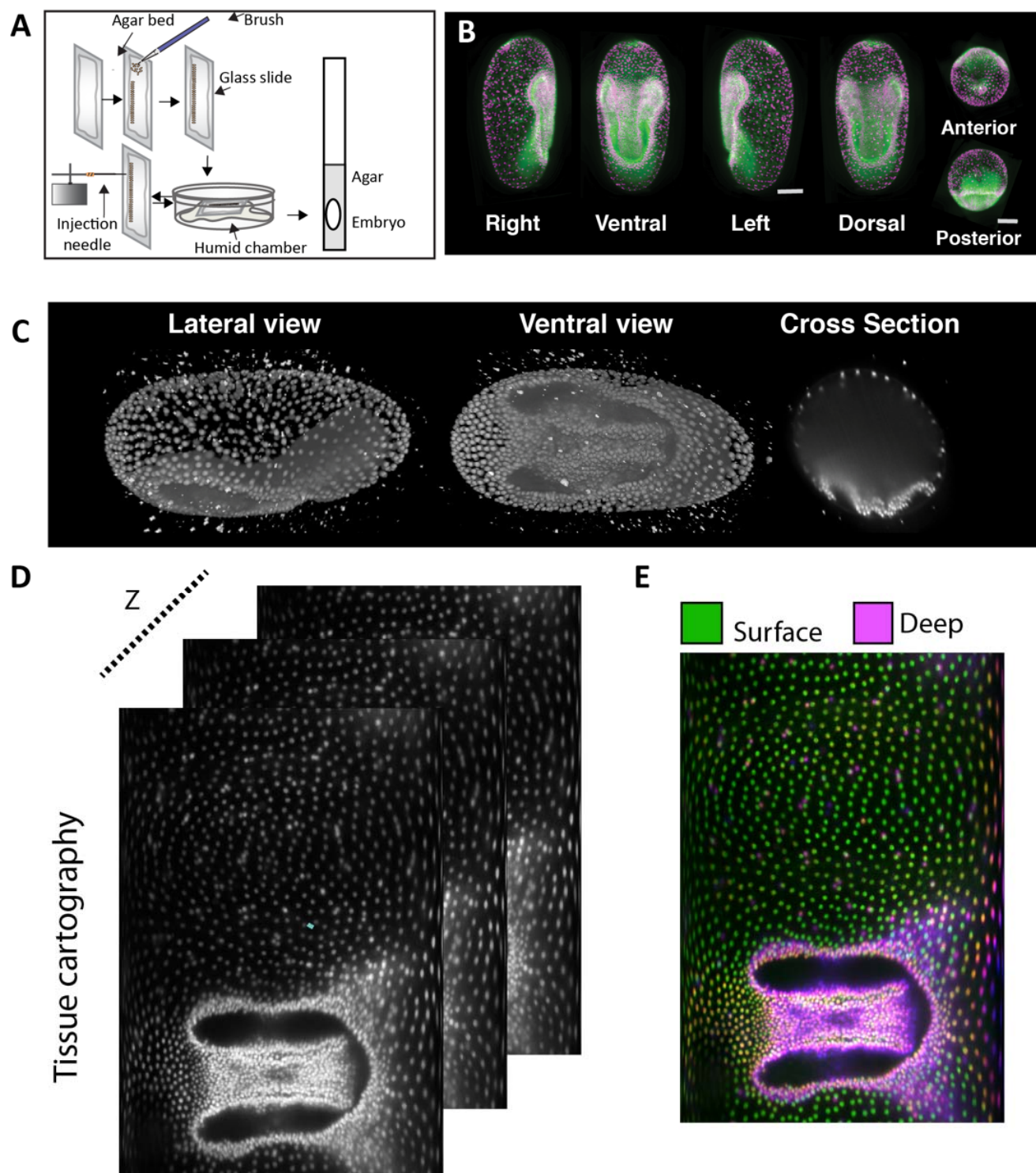
(E) Cartographic projections of a multiview SPIM recording in which embryos injected with Gap43-eYFP and *Tc-zen1* dsRNA was imaged from 5 angles every 5 minutes.

(F) Cartographic projections shown in (E) segmented and colored according to the apical area of the segmented serosa cells.

(G) Cartographic projections shown in (E) segmented and colored according to the shape index of the segmented serosa cells.

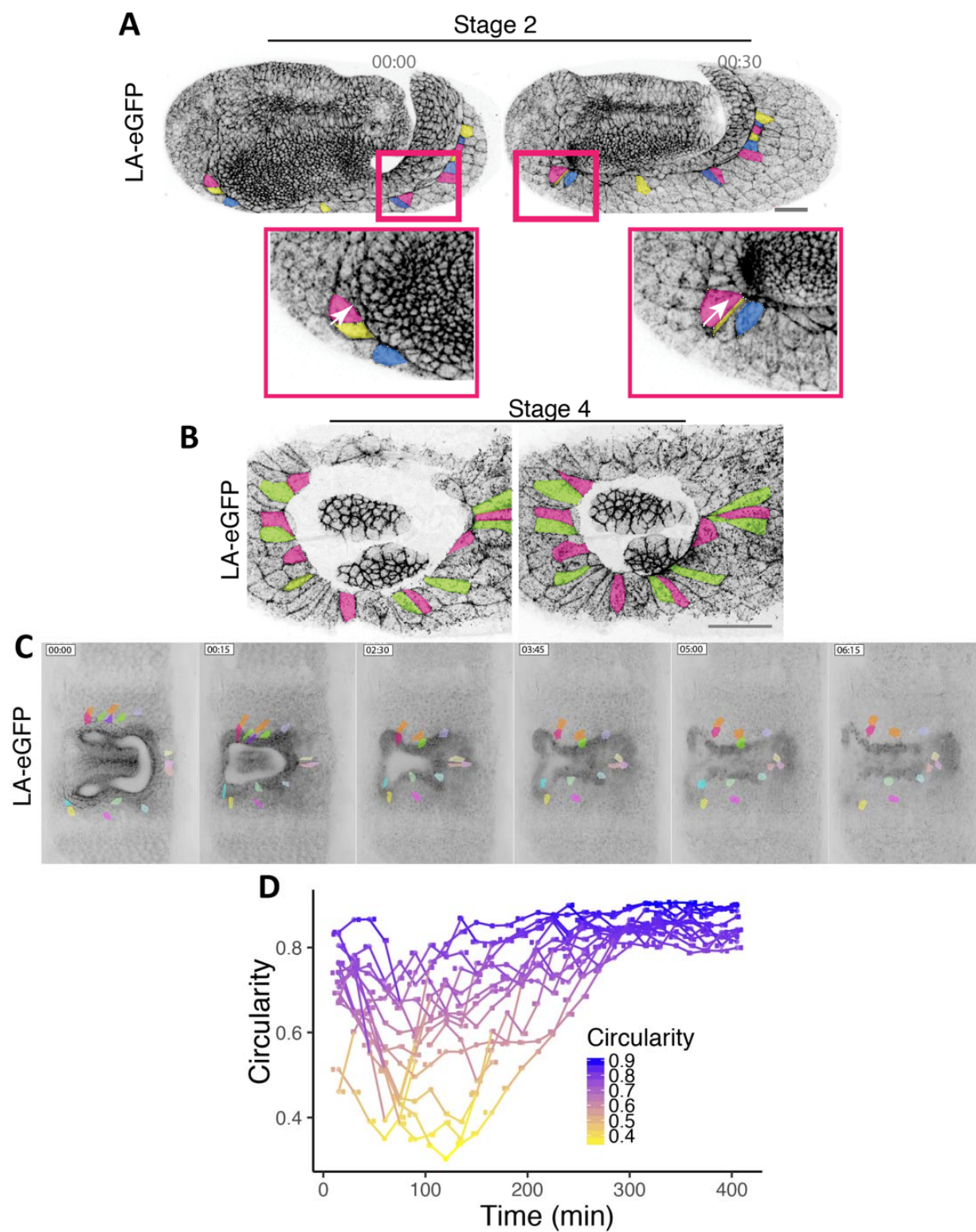
(H) The distributions of shape indices wildtype and *Tc-zen1* knockdown embryos sampled from confocal datasets in the ventral (H) and dorsal (I) serosa regions at Stage 3. The differences in distributions were tested using t-test and p-values between 0.009-0.001 are labelled with \*\*.





## **Supplementary Figure 1: Imaging and image analysis pipeline to study *Tribolium* serosa tissue morphogenesis**

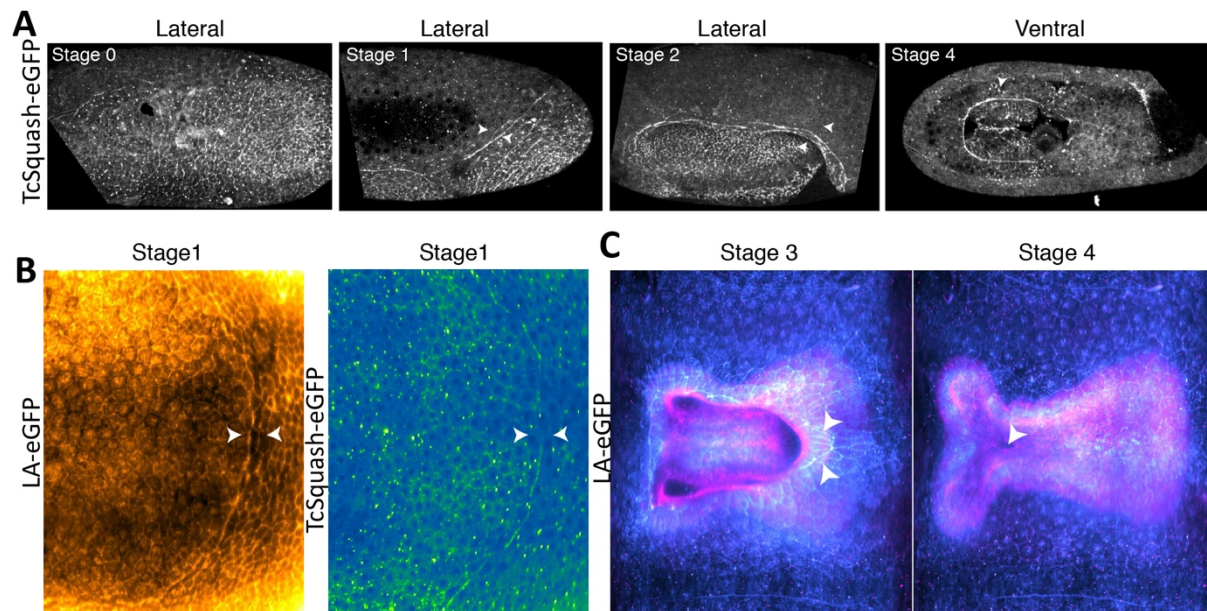
- (A)** Illustration outlines the micro-injection and sample mounting protocol to label *Tribolium* embryos and mount them for lightsheet microscopy.
- (B)** Maximum intensity projections from different orientation of 3D images of embryos injected with LifeAct-eGFP and Hist-RFP. The embryo was imaged from 5 views with a light sheet microscope. Individual view stacks were registered and fused using Fiji Multiview Reconstruction plugin.
- (C)** 3D rendering of Hist-eGFP expressing *Tribolium* embryo reconstructed from multiview SPIM data and viewed from the ventral and lateral side. Sagittal cross section of the same embryo volume.
- (D)** The embryo shown in C is dimensionality reduced from 3D to 2D generating a cartographic projection. Successive, increasingly deep concentric layers of the embryo surface are shown as separate maximum intensity projections.
- (E)** The different layers generated in (D) are color coded to separate the superficial serosa from the internalized embryo.



**Supplementary Figure 2: Anisotropy of the cells at the leading edge of the serosa window increases over time and decreases once they leave the edge**

- (A) Inverted confocal images of Life-Act-eGFP expressing *Tribolium* embryos show selected cell outlines at the leading edge of the serosa window at Stage 2. Insets zoom in on regions highlighted with red boxed. Arrow points to a cell elongating along the axis roughly perpendicular to the leading edge.
- (B) Inverted confocal images of Life-Act-eGFP expressing *Tribolium* embryos show selected elongated cell outlines at the leading edge of the serosa window at Stage 4.
- (C) Inverted, 2D-map-projected confocal images of Life-Act-eGFP expressing *Tribolium* embryos show outlines of selected anisotropically elongated cells during serosa window closure. The highlighted cells increase their shape anisotropy over time till they leave the leading edge of the serosa window and become hexagonal.
- (D) Graph shows the change in circularity of cells highlighted in (C) over time. Circularity is measured as a ratio of the area of the observed nucleus to the area of a circle that has the same perimeter as the observed nucleus.





### Supplementary Figure 3: Actomyosin localization at the embryo-serosa boundary

(A) Myosin localization in *Tribolium* embryo at different stages of gastrulation morphogenesis. Arrowheads point to the myosin cable. The embryos were injected with mRNA encoding Tc-sqh-eGFP and imaged with point scanning confocal microscope.

(B) Images show the dorsal region of Stage 1 embryo from a cartographic projection. The embryo was labeled with LifeAct-eGFP or Tc.sqh-eGFP and imaged with multiview SPIM. Arrows mark the actomyosin enrichment at the border between serosa and embryo (tissue identities inferred by backtracking the time lapse movie).

(C) Images show the ventral region of Stage 3 and 4 embryo from a cartographic projection. The embryo was labeled with LifeAct-eGFP and imaged with multiview SPIM. The different layers of the cartographic projection are colored cyan for surface serosa and magenta for internal embryo layers. The arrowheads point to the actin cable which is lagging behind the serosa window leading edge at Stage 3.

## Supplementary movies

**Supplementary Movie 1:** Lateral and ventral views of 3D rendered multiview Lightsheet recording of *Tribolium* embryo collected from a Hist-eGFP transgenic line. The embryo was imaged from 5 angles at 1.5 minute time interval at 22°C. Time is indicated in hours.

**Supplementary Movie 2:** The expanding serosa is outlined on a 2D cartographic projection of a 4D SPIM recording of a transgenic embryo from the EFA-nGFP line marking cell nuclei. The color of the serosa changes according to its increasing total area. Time is indicated in hours.

**Supplementary Movie 3:** 4D multiview lightsheet recording of a *Tribolium* embryo expressing EFA-nGFP nuclear marker projected as a 2D cartographic map. The embryo was imaged from 5 angles and at 90 seconds time interval. Successive onion layers of the map are color coded to distinguish deeper embryo layers from the superficial serosa. The last few cells contributing to the serosa window closure are tracked from Stage 1 onwards. Time is indicated in hours.

**Supplementary Movie 4:** Timelapse video shows Stage 4 to serosa window closure in a LifeAct-GFP labelled embryo imaged with point scanning confocal microscope. Selected cells at the cable are highlighted and tracked. Time is indicated in hours.

**Supplementary Movie 5:** *Tribolium* embryo labelled with LifeAct-eGFP was imaged using 4D multiview lightsheet microscopy and projected as a cartographic map. Dots and lines show serosa two groups of cells on the dorsal and ventral side of the embryo tracked overtime using Mastodon Fiji Plugin. Time is indicated in hours.

**Supplementary Movie 6:** Cartographic projection of 4D multiview lightsheet recording of an embryo injected with Tc-sqh-eGFP at 22°C. The dorsal part of the embryo is positioned in the middle to show the emergence of the myosin cable at Stage 1 (pointed out by an arrow). Time is indicated in hours.

**Supplementary Movie 7:** Timelapse videos of Stage 1, 3 and 4 embryos labelled with LifeAct-eGFP. The edges of serosa leading edge cells facing the serosa window (where cable like action enrichment occurs) were laser ablated and the edges were tracked with Fiji to measure the recoil velocity over time. Time is indicated in minutes.

**Supplementary Movie 8:** Timelapse video of a Stage 4 transgenic embryo labelled with Tc.sqh-eGFP and imaged with a point scanning confocal microscope and the 3D stacks were maximum intensity projected. Myosin is distributed in a heterogeneous manner along the cable with different cell edges showing different intensities (highlighted using Green-Blue look-up table; green is high myosin). Time is indicated in minutes.

**Supplementary Movie 9:** Timelapse video of an embryo labelled with LifeAct-eGFP in which *Tc-zen1* was knocked down using parental RNAi. The embryo was imaged with a point

scanning confocal microscope and the 3D stacks were maximum intensity projected. Time is indicated in hours.

**Supplementary Movie 10:** Cartographic projection of a multiview Lightsheet dataset. The embryo was injected with mRNA for GAP43-eYFP to label cell membranes and dsRNA to knockdown *Tc-zen1*. Time is indicated in hours.